Development of Urinary Biomarkers for Internal Exposure by Cesium-137 Using a Metabolomics Approach in Mice

Author(s): Maryam Goudarzi , Waylon Weber , Tytus D. Mak , Juijung Chung , Melanie Doyle-Eisele , Dunstana Melo , David J. Brenner , Raymond A. Guilmette and Albert J. Fornace
Source: Radiation Research, 181(1):54-64. 2013.
Published By: Radiation Research Society
DOI: http://dx.doi.org/10.1667/RR13479.1
URL: http://www.bioone.org/doi/full/10.1667/RR13479.1

RADIATION RESEARCH **181**, 54–64 (2014)
0033-7587/14 $15.00

DOI: 10.1667/RR13479.1

Development of Urinary Biomarkers for Internal Exposure by Cesium-137 Using a Metabolomics Approach in Mice

Maryam Goudarzi,[a] Waylon Weber,[b] Tytus D. Mak,[c] Juijung Chung,[a] Melanie Doyle-Eisele,[b] Dunstana Melo,[b] David J. Brenner,[d] Raymond A. Guilmette[b] and Albert J. Fornace Jr.[a,c,1]

[a] *Biochemistry and Molecular and Cellular Biology, Georgetown University, Washington DC;* [b] *Lovelace Respiratory Research Institute, Albuquerque, New Mexico;* [c] *Lombardi Comprehensive Cancer Center, Georgetown University, Washington DC; and* [d] *Center for High-Throughput Minimally-Invasive Radiation Biodosimetry, Columbia University, New York, New York*

Goudarzi, M., Weber, W., Mak, T. D., Chung, J., Doyle-Eisele, M., Melo, D., Brenner, D. J., Guilmette, R. A. and Fornace Jr., A. J. Development of Urinary Biomarkers for Internal Exposure by Cesium-137 Using a Metabolomics Approach in Mice. ***Radiat. Res.*** **181, 54–64 (2014).**

Cesium-137 is a fission product of uranium and plutonium in nuclear reactors and is released in large quantities during nuclear explosions or detonation of an improvised device containing this isotope. This environmentally persistent radionuclide undergoes radioactive decay with the emission of beta particles as well as gamma radiation. Exposure to ^{137}Cs at high doses can cause acute radiation sickness and increase risk for cancer and death. The serious health risks associated with ^{137}Cs exposure makes it critical to understand how it affects human metabolism and whether minimally invasive and easily accessible samples such as urine and serum can be used to triage patients in case of a nuclear disaster or a radiologic event. In this study, we have focused on establishing a time-dependent metabolomic profile for urine collected from mice injected with ^{137}CsCl. The samples were collected from control and exposed mice on days 2, 5, 20 and 30 after injection. The samples were then analyzed by ultra-performance liquid chromatography coupled to time-of-flight mass spectrometry (UPLC/TOFMS) and processed by an array of informatics and statistical tools. A total of 1,412 features were identified in ESI$^+$ and ESI$^-$ modes from which 200 were determined to contribute significantly to the separation of metabolomic profiles of controls from those of the different treatment time points. The results of this study highlight the ease of use of the UPLC/TOFMS platform in finding urinary biomarkers for ^{137}Cs exposure. Pathway analysis of the statistically significant metabolites suggests perturbations in several amino acid and fatty acid metabolism pathways. The results also indicate that ^{137}Cs exposure causes: similar changes in the urinary excretion levels of taurine and citrate as seen with external-beam gamma radiation; causes no attenuation in the levels of hexanoylglycine and N-acetylspermidine; and has unique effects on the levels of isovalerylglycine and tiglylglycine.

INTRODUCTION

Cesium-137 (^{137}Cs) is one of the most feared fission radionuclides in nuclear reactors as it can easily spread in water and air after an explosion, and decays by high-energy pathways. With a half-life of 30 years, 95% of the released ^{137}Cs decays to ^{137m}Ba barium-137 by beta emission, which in turn decays in 150 s by gamma emissions to stable ^{137}Ba. The Chernobyl accident and to a lesser extent the Goiania scrap metal and Fukushima Daiichi accidents are evidence to the historical notoriety of ^{137}Cs (*1*). The persistency of ^{137}Cs in soil and water decades after the Chernobyl accident and recently in Fukushima Daiichi calls for better screening of exposure to ^{137}Cs and predicting the health risks in the disaster zones. Research and industrial gamma irradiators frequently contain ^{137}Cs, which also raises concern for terrorist use in a radiological dispersal device. Therefore, our team has focused on identifying ^{137}Cs-induced metabolic pathway perturbations in easily accessible biofluids such as urine, which can help triage people in case of a radiologic or nuclear incident.

In this study we took advantage of the superior sensitivity that mass spectrometry has to offer in detecting even small changes in the urinary excretion levels of metabolites after ^{137}Cs exposure in mice. The absorbed doses ranged from about 2–10 Gy during the 30-day time course and were chosen to include those associated with acute radiation injury, up to and above the LD50. The overall metabolomic profile of the urine from mice exposed to ^{137}Cs was mapped out by using an array of bioinformatics tools and compared to urine from control mice to determine statistically significant changes that may be used as early markers of exposure. The changes in the urinary metabolome of the mice over time indicate which pathways are the most

Editor note. The online version of this article (DOI: 10.1667/RR13479.1) contains supplementary information that is available to all authorized users.

[1]Address for correspondence: Georgetown University, Lombardi Comprehensive Cancer Center, Reservoir Road, Washington, DC 20057; e-mail: af294@georgetown.edu.

affected as a result of ^{137}Cs exposure. Furthermore, the selected significant ^{137}Cs exposure markers were compared to known external-beam γ irradiation (henceforth referred to as γ irradiation in this article) markers to determine similarities between the two types of exposures.

There are several radiobiological considerations regarding the use of the internally deposited radionuclide ^{137}Cs to deliver radiation dose compared with the more typical application of external beams of X rays or gamma rays. First the distribution of radiation dose in a mouse model is relatively uniform both for internally deposited ^{137}Cs and for external photon beam radiation. However, the temporal dose patterns for these two types of radiation exposure differ significantly. For acute external-beam irradiation, dose rates are often in the range of 500–1,000 mGy/min. By contrast, the initial dose rate for the amount of ^{137}Cs used in this study was about 3 mGy/min, and this dose rate decreased by about twenty-fold by 28 days, the end of the irradiation period. It is well recognized that dose rate can affect the magnitude and type of biological effects resulting from such irradiation. However, potentially equally important are the effects of changes in dose rate during the dose delivery. How this rapid decrease in dose rate influences the measured end points is unknown, and is one of the central questions to be addressed. It is recognized that the results from this single study will not be adequate to fully sort out the relative effects of dose, dose rate and dose-rate changes.

MATERIALS AND METHODS

Chemicals

Debrisoquine sulfate, 4-nitrobenzoic acid (4-NBA), xanthurenic acid, hippuric acid, urocanic acid, citric acid, α-ketoglutaric acid, β-hydroxyisovaleric acid, uric acid, isethionic acid and taurine were purchased from Sigma-Aldrich (St. Louis, MO). O-Propanoylcarnitine[chloride] and isovalerylglycine were obtained from Fisher Scientific (Hanover Park, IL). Methylguanine was obtained from Tokyo Chemical Industry Co., LTD (Tokyo, Japan). The UPLC-grade solvents were purchased from Fisher Scientific (Hanover Park, IL).

Animals

Animal studies were approved by the Lovelace Biomedical and Environmental Research Institute (LBERI) Institutional Animal Care and Use Committee; conducted in facilities accredited by the Association for Assessment and Accreditation of Laboratory Animal Care International; and carried out in compliance with the *Guide for the Care and Use of Laboratory Animals* (National Research Council 1996). Eighty-four male C57Bl/6 mice aged 10–12 weeks with an average weight of 27.5 grams were obtained from Charles River Laboratories (Frederick, MD). The mice were quarantined at LBERI for 14 days prior to the start of the study. Each mouse was injected intraperitoneally (i.p.) with 50 μL of 8.0 ± 0.3 MBq ^{137}CsCl solution. As a note, the intraperitoneal route of administration was selected for convenience, as it has been demonstrated experimentally that the dosimetric biokinetics of ^{137}Cs is very similar whether the soluble compound is administered by intravenous, intraperitoneal or inhalation routes (*2*). ^{137}CsCl injected mice were then housed individually in microisolator cages, which were separated by lead shielding to minimize cross-irradiation. The control animals were left untreated and housed four mice per cage. The mice had access to Teklad Certified Global Rodent Diet 2016 (Harlan Teklad Madison, WI) and water except during dose administration and whole-body *in vivo* counting.

Dose Calculations

The ^{137}Cs retention measurements *in vivo* were obtained by serial counting for each mouse during the experiment using the LBERI *in vivo* photon counting system, which consisted of a single 5 inch diameter Phoswich [dual NaI(Tl) – CsI(Tl) detector] and associated pulse height analysis electronics. The whole-body retention data from each mouse were fitted to one- or two-component negative exponential functions, depending on when the mouse was sacrificed (short times only provided enough data for one-component fitting). The average whole-body retention of i.p.-injected ^{137}Cs in mice was determined to be:

$$R(t) = 21.5e^{-1.0t} + 78.5e^{-0.096t}$$

where R(t) is expressed as percentage of the injected dosage of ^{137}Cs, and t is in days. The respective retention half times were 0.7 days and 7.2 days.

To convert the empirical ^{137}Cs retention data into radiation absorbed dose, specific absorbed fractions for electrons and photons published by Stabin *et al*. (*3*), and which were developed specifically for young adult mice and rats, were converted into a dose coefficient (dose in Gy per unit decay of ^{137}Cs in equilibrium with ^{137m}Ba), and integrated over the experimental lifespan for each individual mouse. Since the biological distribution of ^{137}Cs and its absorbed radiation dose pattern is relatively uniform throughout the body, only the whole-body dose was calculated and used for this study.

To convert the empirical ^{137}Cs retention data into radiation absorbed dose, the software RATDOSE (*4*) was used. This program uses specific absorbed fractions published by Stabin *et al*. (*3*), which were developed specifically for young adult mice and rats, to convert the deposition of photon and electron energy from the radioactive decay of ^{137}Cs and its radioactive progeny ^{137m}Ba (assumed to be in secular equilibrium with the parent ^{137}Cs) into absorbed radiation dose in Gy. Since the biological distribution of ^{137}Cs is relatively uniform throughout the body, only the whole-body dose was calculated and used for this study.

Urine Collection

Lovelace: Urine was collected 2, 3, 5, 20, and 30 days post-injection. Mice at each time point were sacrificed with i.p. injection of Euthasol (1:9 dilution with sterile saline) and urine was collected from the bladder of each mouse at necropsy with a syringe and needle. As a result the number of urine samples collected from mice at each time point varied, however this article focuses on the time points that contained at least five biological replicates (Table 1). Because only three urine samples could be collected from mice 3 days post-injection, this time point was eliminated from the study. Urine samples collected from control mice at days 20 and 30 were combined to increase the number of biological replicates at these times. Urine samples from control mice at days 2 and 3 were combined for the same reason (Table 1).

Sample Preparation and Mass Spectrometry Analysis

Urine samples were prepared as described previously by our group (*5*). Briefly, urine was diluted 1:4 in a 50% acetonitrile solution containing 30 μ*M* of 4-nitrobenzoic acid and 2 μ*M* of debrisoquine. The samples were centrifuged at maximum speed to precipitate out the proteins. A 5 μL aliquot of the recovered supernatant was then injected into a reverse-phase 50 × 2.1 mm Acquity 1.7 μm C18 column (Waters Corp, Milford, MA) coupled to a time of flight mass spectrometry (TOFMS). The 10-min long mobile phase gradient

TABLE 1
Number of Mice at each Urine Collection Time Point along with Cumulative Doses Estimated at each Time Point

Treatment group	Time point	Number of mice	Cumulative average dose (Gy)
Control	Day 2	8	–
	Day 5	6	–
	Day 20	5	–
	Day 30	5	–
^{137}Cs exposed	Day 2	5	1.95
	Day 5	5	4.14
	Day 20	8	9.46
	Day 30	5	9.91

switched from 100% aqueous solvent to 100% organic at a flow rate of 0.5 mL/min. The QTOF Premier mass spectrometer was operated in positive (ESI^+) and negative (ESI^-) electrospray ionization modes. The MS data were acquired in centroid mode and processed using MassLynx software (Waters Corp, Milford, MA).

Data Processing

As described previously (*4*) MarkerLynx software (Waters Corp, Milford, MA) was used to construct a data matrix consisting of the retention time, *m*/*z*, and abundance value (by the normalized peak area) for each ion using the raw MS chromatograms. The abundance value of each ion was normalized as a ratio of the total ion count (TIC) of creatinine at *m*/*z* of 114.0667 ($[M+H]^+$) and retention time of 0.32 min in each sample. Creatinine normalization has been utilized in our previous studies and deemed appropriate as the total excretion of creatinine remains relatively unchanged in IR-exposed mice when compared to control mice (11 and supplementary material Fig. S2A; http://dx.doi.org/10.1667/RR13479.1.S1). In-house statistical analysis programs along with SIMCA-P^+ (Umetrics, Umea, Sweden) and Random Forests (RF) were utilized during this analysis. SIMCA-P^+ was utilized to evaluate the entire data matrix in an unsupervised and holistic manner as described previously (*5*). Briefly, the data was Pareto scaled to increase the importance of low abundance ions prior to unsupervised PCA analysis. This step was critical in that it revealed global trends in the data that gave direction to the more targeted analyses by our in-house program. This program allowed extraction of the ions with nonzero abundance values, which were detected in at least 70% of samples in each study group. Data were then log-transformed and analyzed for statistical significance by the nonparametric Mann-Whitney U statistical hypothesis test ($P < 0.05$). Statistical significance testing for ions with nonzero abundance values in at least 70% of the samples in only one group were analyzed as categorical variables for presence status (i.e., nonzero abundance) by Fisher's exact test ($P < 0.05$). The log-transformed data for statistically significant full-presence ions was then utilized for principal component analysis (PCA) by singular value decomposition for the purpose of data visualization. Lastly, RF was employed to confirm the results by constructing 10,000 trees with variable importance over 25 independent random forests. Multidimensional scaling (MDS) plots were created using the top 20 ranked ions to achieve the highest classification accuracy. Heat maps were generated on the top 100 ranked ions, grouped by treatment and the metabolites hierarchically clustered by complete linkage using Euclidian distance.

Metabolic Pathway Analysis

Statistically significant ions were putatively identified by in-house software, which utilizes the Human Metabolome Database (HMDB), and the Kyoto Encyclopedia of Genes and Genomes (KEGG) database (*6*). The *m*/*z* values were used to putatively assign IDs to the ions by neutral mass elucidation, which was accomplished by considering the possible adducts, H^+, Na^+ and/or NH_4^+ in the ESI^+ mode, and H^- and Cl^- in the ESI^- mode. The masses were then compared to the exact mass of small molecules in the databases, from which putative metabolites were identified with a mass error of 20 parts per million (ppm) or less. KEGG annotated pathways associated with these putative metabolites were also identified. Selected metabolites from these pathways were later validated by tandem mass spectrometry (MS/MS) as described below.

MS/MS Validation of Select Metabolites

Putative identities of the selected metabolites were determined using online databases as mentioned above within a predefined mono-isotopic mass error window of 7 ppm. The retention time of each metabolite was considered to narrow down the possibilities of the putative identifications. Several of the putatively identified statistically significant metabolites ($P < 0.05$, Mann-Whitney U test) were then chosen based on their biological relevance for further MS/MS validation against commercially available pure standards. A Q-Tof Premier™ MS with ramping collision energy between 5–55 eV was used to create an MS/MS fragmentation pattern for the selected metabolites, which were then compared to that of pure chemicals for validation purposes. In the case of O-propanoylcarnitine, the pure standard was spiked in a urine sample for compound stabilization and to create the same matrix effect as seen in the biological samples. As for the ion $[M+H]^+ = 244.1546$, HMDB was initially used to putatively identify it as tiglylcarnitine within a 7 ppm mass error window. However we could not commercially obtain a pure chemical standard for this metabolite. Therefore, online databases and Pubmed were utilized to predict the MS/MS spectrum of tiglylcarnitine. Acylcarnitine species are known to give rise to two distinct daughter ions in ESI^+ mode at *m*/*z* of 85 and 144 due to McLafferty rearrangement (*7*). This is represented by cleavage at sites 1 and 2 in supplementary material Fig. S4; http://dx.doi.org/10.1667/RR13479.1.S1. These fragments are characteristic of acylcarnitines and are routinely used to identify them in urine and serum (*8*). In addition to these two fragments, the loss of carnitine group with *m*/*z* of 161 as described in ref. (*7*) and depicted by cleavage 3 in supplementary material Fig. S4 is also one of the expected fragments. The acyl group of tiglylcarnitine was predicted to produce a fragment at *m*/*z* of 185 as depicted by cleavage 1 in supplementary material Fig. S4 after the loss of quaternary ammonium moiety with *m*/*z* of 59. Furthermore, the loss of quaternary ammonium group and the carboxyl group (COO^-) of the carnitine moiety can produce a fragment at *m*/*z* 135. The peak at *m*/*z* of 201 is believed to be due to the loss of the carboxyl group. After calculating the *m*/*z* of the expected daughter ions, the spectral feature at $[M+H]^+ = 244.1546$ was fragmented using collision energy of 7 eV. The resulting MS/MS spectrum was then compared against the calculated fragments mentioned above from which the chemical structure of tiglylcarnitine was elucidated. The obtained MS/MS spectrum was also investigated for the spectral features published in ref. (*9*) for further confirmation.

RESULTS

We used a variety of statistical tools to model and evaluate the unique urinary metabolomic signature of ^{137}Cs-exposed mice as explained below. PCA on the full dataset was first conducted in SIMCA-P^+ to determine overall differences in the urinary metabolomic signatures of control and ^{137}Cs exposed mice. Figure 1A shows that even with a completely unsupervised methodology, differentiation between the two groups using the abundances of 747 ions in the ESI^+ mode was evident. With the exception of one urine

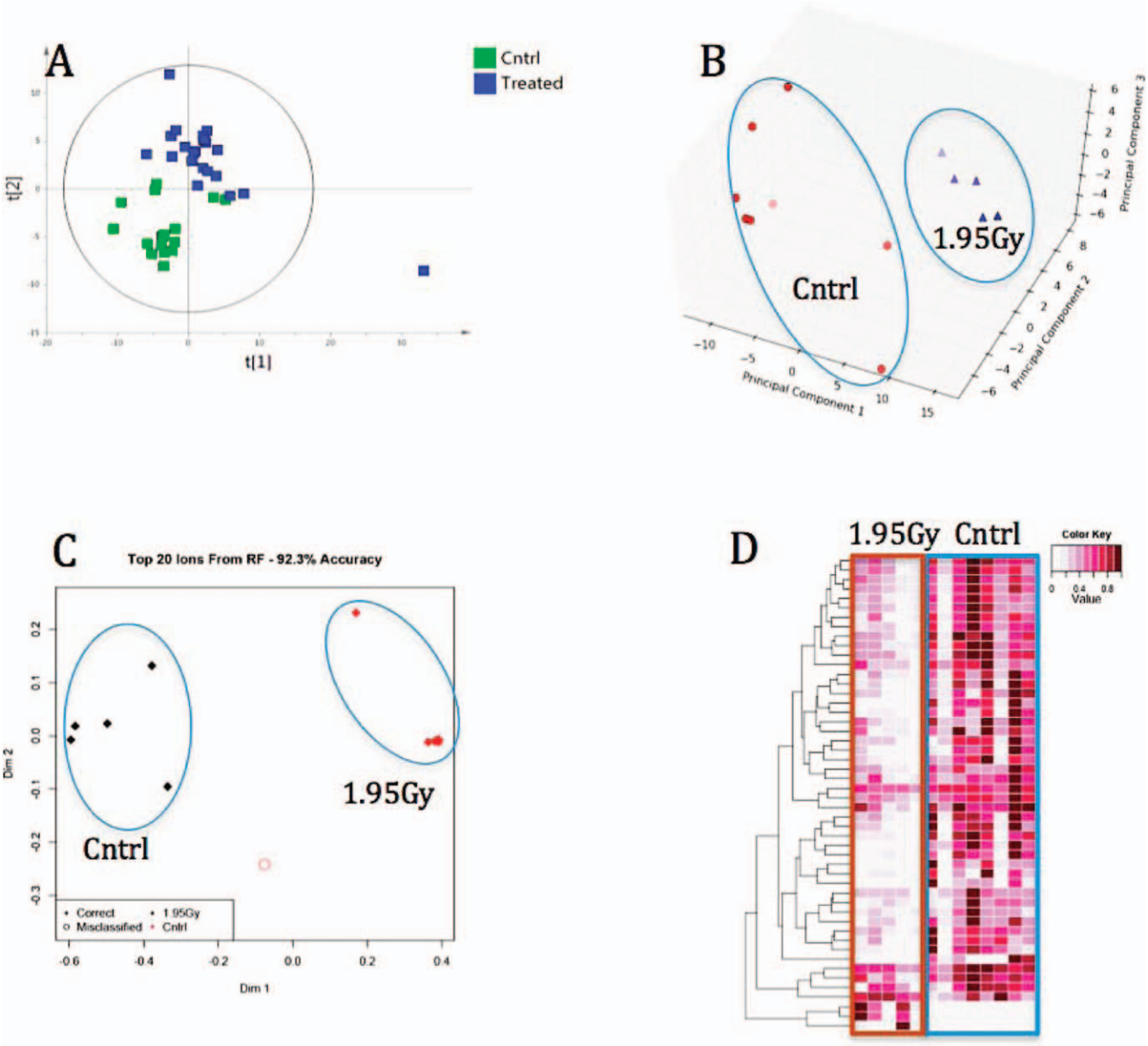

FIG. 1. The urinary metabolomic profile of ^{137}Cs-exposed mice shows significant separation from that of control mice in ESI$^+$ mode. Panel A: PCA conducted on the full dataset generated in SIMCA-P$^+$ showing the separation of the urinary metabolomic signatures of control mice (at all time points) and ^{137}Cs-exposed mice (at all time points). Panel B: PCA conducted only on data from statistical significant ions. Panel C: Random-Forests-created multidimensional scaling (MDS) plot both depicting visible separation of metabolomic profiles using the top statistically significant metabolites. Each red circle or diamond represent a urine sample collected from a mouse in the ^{137}Cs-exposed group and each black dot or diamond is a urine sample collected from a mouse in the control group. Panel D: Random Forests-created heatmap of the top ranked 100 ions grouped by treatment and hierarchically clustered using Euclidian distance.

sample from a ^{137}Cs-exposed mouse, the rest of the exposed samples clustered together and were distinguishable from the control mice on the second component (t[2]) of the PCA score scattered plot.

Moreover, urine samples from ^{137}Cs-exposed mice were divided into 4 groups based on post-exposure urine collection date (Table 1). Each time point was then compared to its corresponding control samples to determine time point and cumulative dose-specific metabolomic signature. When conducting PCA on only the statistically significant subset of ions at day 2 post-exposure, the urinary metabolomic profile of ^{137}Cs-exposed mice was well separated from that of the corresponding control mice as shown in Fig. 1B. RF was later used to further confirm the separation of the metabolomic signature of day 2 after ^{137}Cs-exposure from that of control mice. The proximity matrix based multidimensional scaling (MDS) plot (Fig. 1C) shows that the metabolomic signatures can be separated with 92% accuracy using only the 20 ions with the highest variable importance. Therefore, RF along with the aforementioned

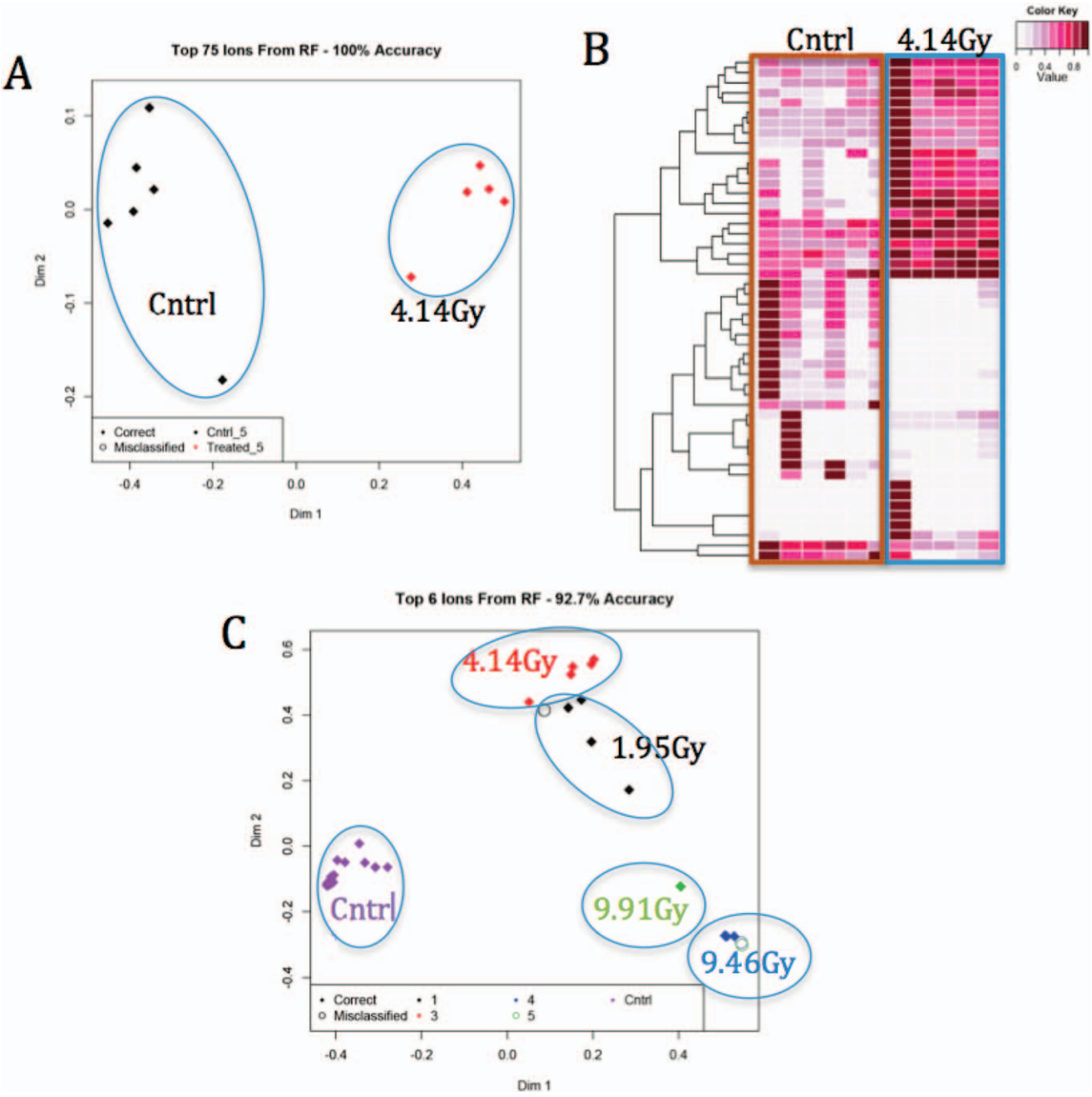

FIG. 2. Separation of metabolomic signatures of ^{137}Cs-exposed and control mice becomes more evident at later time points, which correlates to higher cumulative doses. A) RF generated MDS plot and B) heatmap show a clear separation of metabolomic profile of day-5 urine samples from that of control urine samples. C) Distinct changes in the metabolomic profile of urine from mice at different doses lead to the separation of the profiles as shown in this RF-generated MDS plot with the top ranked 6 ions.

statistical tools establishes a unique metabolomic signature for early ^{137}Cs exposure. Figure 1D shows the RF-created heatmap of the top ranked 100 ions with the most variable importance, which were grouped by treatment and hierarchically clustered by Euclidian distance. This heatmap depicts a clear separation between the urinary metabolomic signature of exposed and control mice 2 days post-exposure.

The results indicate that ^{137}Cs causes sufficient pathway perturbations in mice that even as early as 2 days post-exposure and at as low as 1.95 Gy exposure the urinary metabolomic profile of mice changes significantly and is easily distinguishable from that of control mice. The same statistical tools were employed to study the differences in the urinary metabolome of mice at 5, 20 and 30 days post-exposure and respective doses of 4.14, 9.46 and 9.91 Gy. At higher cumulative doses the separation becomes more evident. For instance, Fig. 2A shows that at 4.14 Gy (day 5) the metabolomic profiles could be separated with higher

TABLE 2.
Selected Urinary Metabolite Markers of ^{137}Cs Exposure

Sample no.	KEGG ID	Description (generic name)	ESI Mode	Observed m/z_RT	Fold change (Cs/Cntrl)*			
					D2	D5	D20	D30
1	C02470	Xanthurenic acid*	POS	206.045_1.4388	0.51	0.63	0.56	0.58
2	–	Unknown	POS	162.0551_3.0656	0.40	0.46	0.21	0.24
3	–	Unknown	POS	338.0862_0.5976	0.47	0.55	0.64	0.68
4	–	Tiglylcarnitine†	POS	244.1546_3.3977	0.18	0.14	0.14	0.13
5	LMFA07070001	Hexanoylcarnitine*	POS	260.1862_3.2675	0.33	0.63	0.73	0.64
6	–	Tiglylglycine*	POS	180.0659_1.9485	1.22	3.05	2.24	1.89
7	C00407	Isoleucine/Leucine*	POS	132.0881_0.3049	0.81	0.76	0.53	0.53
8	–	Unknown	POS	166.0724_0.3294	1.25	1.21	1.25	1.26
9	–	β-hydroxyisovaleric acid*	POS	119.0497_2.0681	1.19	1.51	1.54	1.90
10	C01586	Hippuric acid*	NEG	178.0502_1.9084	5.75	2.69	2.91	1.88
11	_	Isovalerylglycine*	NEG	158.0817_1.5374	0.90	0.83	0.79	0.75
12	C00158	Citrate*	NEG	191.0187_0.3418	0.31	0.63	0.86	0.94
13	–	Unknown	NEG	206.0459_1.9205	0.39	0.62	1.72	2.33
14	C00366	Uric qcid*	NEG	167.0201_0.3246	0.93	0.87	2.50	1.54
15	C00245	Taurine*	NEG	124.0067_0.2971	1.75	1.88	5.19	1.31
16	–	N-Acetyltaurine	NEG	166.0174_0.324	1.66	1.33	1.82	1.02
17	C05123	Isethionic acid*	NEG	124.9917_0.3236	1.92	1.95	2.58	1.39
18	C00026	α-Ketoglutaric acid*	NEG	145.014_0.3193	0.72	0.68	0.81	0.86

Notes. Asterisks represent those metabolites that were validated by tandem MS/MS in this study. *Designated metabolites whose identities were confirmed by tandem MS. †Designates tiglylcarnitine whose daughter ions were first calculated and compared to known carnitine species prior to MS/MS fragmentation. The fold change after 2, 5, 20 or 30 days was calculated for each metabolite by normalizing the intensity value of a metabolite to that of creatinine in each ^{137}Cs-exposed urine sample and averaging over the technical replicates, then dividing it by the average creatinine normalized intensity value of the same metabolite in the urine of control mice. The values were further normalized to internal standards in each ESI mode.

accuracy (100%) with more metabolites (75) as shown in the RF-generated MDS plot. Furthermore, each cumulative dose creates a unique metabolomic signature distinguishable from that of the other doses and control mice. The top ranked 6 ions can be used to separate the metabolomics profile of each dose from the rest with 92% accuracy as shown in Fig. 2C. Three of these ions have been putatively assigned to guanine ($[M+H]^+ = 325.0889$), hydroxyindolepyruvate ($[M+H]^+ = 220.0637$) and phenylalanine ($[M+H]^+ = 188.0743$) while the identities of the other three could not be assigned.

With the utilization of various statistical tests such as Mann-Whitney U test and Welch's *t* test, we were able to focus our search on the metabolites that contributed most to the separation of metabolomic profiles at different doses/time points. The average ion abundances in each ESI mode were used to select metabolite markers that are dose specific as well as show specific up or down-regulation trends across the doses/time points. Table 2 summarizes several of these metabolites along with the fold changes in their abundances post-injection. The fold changes were calculated by dividing the average urinary abundance of an ion in ^{137}Cs-exposed mice to that of the same ion in the control mice at matched dose/time points.

The ions in Table 2 are also among the top statistically significant in ^{137}Cs exposure, some of which show the same up-regulation trend post-exposure as seen with γ irradiation (supplementary material Table S1; http://dx.doi.org/10.1667/RR13479.1.S2). Among the top abundant ions in the urine of ^{137}Cs-exposed mice were uric acid (167.0201 $[M-H]^-$), taurine (124.0067 $[M-H]^-$), putative N-acetyltaurine (166.0724 $[M-H]^-$) and hexanoylcarnitine (206.1862 $[M-H]^+$). Uric acid, taurine and hexanoylcarnitine were chemically validated by MS/MS. Except for hexanoylcarnitine, the above metabolites showed the same up-regulation pattern as seen with γ irradiation (*10, 11*). The creatinine normalized urinary abundance of uric acid shows a 2.5-fold increase 20 days post-exposure and the urinary abundance levels of taurine show a 1.7-fold increase post-exposure as early as day 2 and up to fivefold at 20 days post-exposure. This is in accordance with previous γ-irradiation studies (*10*). Figure 3 shows the dose response at various time points post-injection for four up-regulated metabolite markers. The urinary excretion levels of isethionic acid, a taurine pathway metabolite, shows similar upregulation trends to taurine. Tiglylglycine (TG) is also among the up-regulated metabolite. TG is a byproduct of isoleucine degradation pathway and is formed by the action of a mitochondrial complex-1 enzyme. The data show that its levels increase up to threefold by day 5 post-exposure at a dose of 4.14 Gy and persist through day 30 post-exposure at a dose of 9.91 Gy. This may indicate a perturbation in the function of mitochondrial complex-1 in response to ^{137}Cs exposure as early as 2 days post-exposure. Another up-regulated ion is 166.0724 *m/z* and retention time of 0.3294. This metabolite was first putatively identified as methylguanine, however its identity could not be validated by MS/MS. Nonetheless, this metabolite shows distinct and

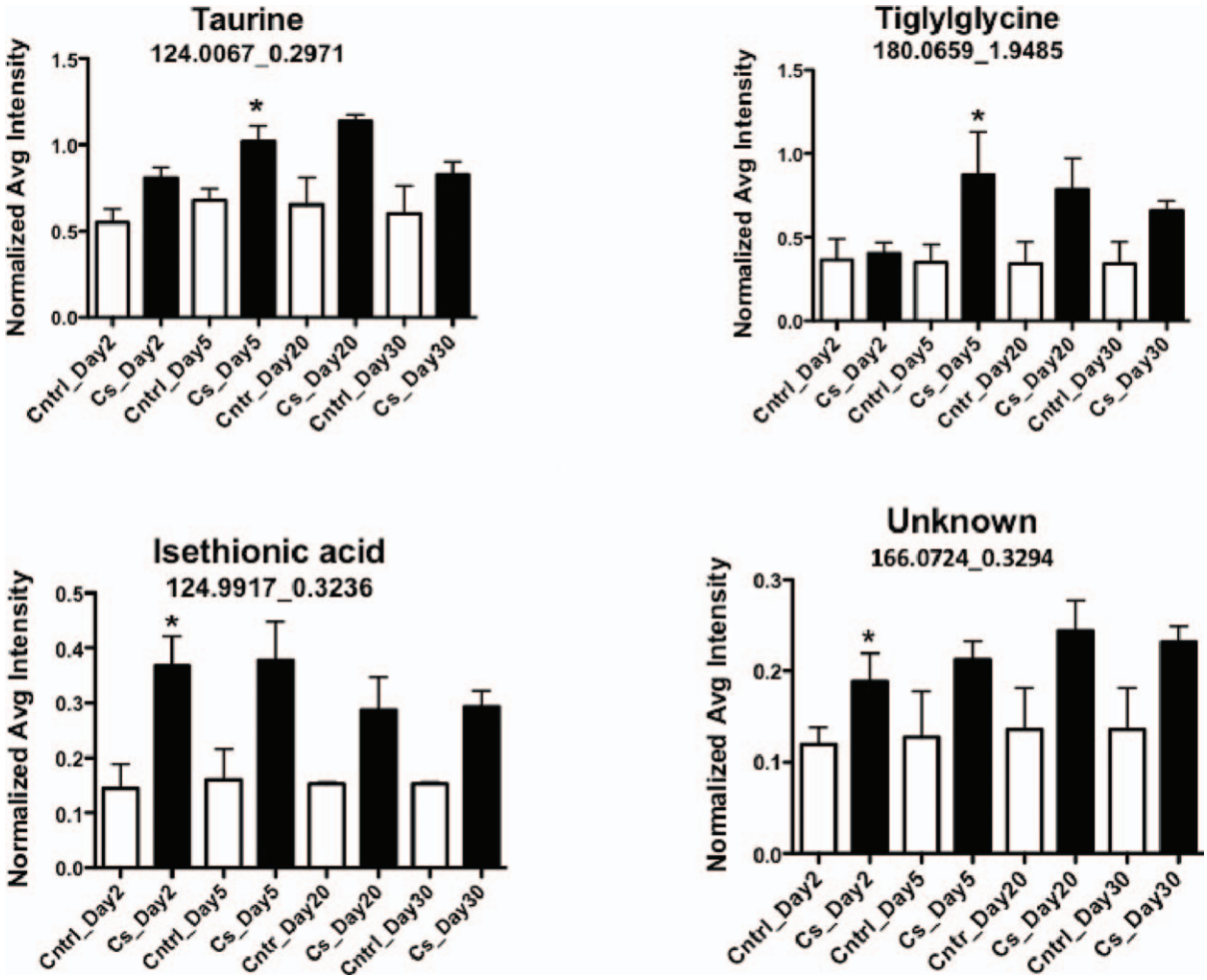

FIG. 3. Urinary excretion abundance of 4 up-regulated metabolite markers in response to ^{137}Cs exposure. Taurine (P value 0.00111) and isethionic acid (P value 0.00291) are from ESI$^-$ mode and tiglylglycine (P value 0.000533) and the unknown ion (P value 0.0306) are from ESI$^+$ mode data. The identities of the ion were validated by tandem MS. The abundance of each metabolite was normalized to total creatinine and internal standards spiked in samples in each ESI mode. *Designates a significant change in the urinary excretion of a metabolite post-irradiation when compared to its urinary excretion in the urine of control mice ($P < 0.05$).

consistent up-regulation in ^{137}Cs-exposed mice and more investigation is needed to determine its identity.

The data was also explored for the presence of down-regulated metabolites of biological importance. Figure 4 shows examples of down-regulated metabolite markers post ^{137}Cs exposure. Chemically identified as xanthurenic acid appeared at half its urinary excretion level in ^{137}Cs-exposed mice 2 days after exposure. Its levels did not recover and remained lower than that in the urine of control mice through day 30 post-exposure. Xanthurenic acid is a metabolite of tryptophan pathway and plays an important role in energy metabolism and aging (*12*).

Tiglylcarnitine (TC) and N-isovalerylglycine (IVG) also show consistent diminishing urinary excretion levels in ^{137}Cs-exposed mice. TC is an organic acid involved in isoleucine degradation pathway and IVG is a metabolite of leucine catabolic pathway. The decrease in the urinary excretion level of IVG post ^{137}Cs exposure is similar to what has been reported in literature (*10*) for external-beam γ irradiation. These observations drove us to look at the levels of leucine and isoleucine in the urine of control and exposed mice. Therefore the spectral feature at m/z of 132.0881 (ion 16 in Table 2) was subjected to MS/MS fragmentation and was compared to that of pure leucine and isoleucine standards. The results showed that these two molecules produce identical MS/MS spectra in our LC/MS system, which made it impossible for us to assign the urinary ion to one of these two molecules based on its MS/MS fragmentation pattern. Thus this down-regulated ion is noted as isoleucine/leucine in Table 2 and throughout this article. In the case of TC, its calculated carnitine moiety daughter ions at CE of 7 eV matched MS/MS spectra of known carnitine species (*7–9*). The calculated fragments of its acyl group were also observed in the MS/MS spectrum of the ion at m/z of 244 extracted from the urine samples as shown in the supplementary material Fig. S4; http://dx.doi.org/10.1667/RR13479.1.S1. Further pathway analysis of the statistically significant ions revealed that the leucine/

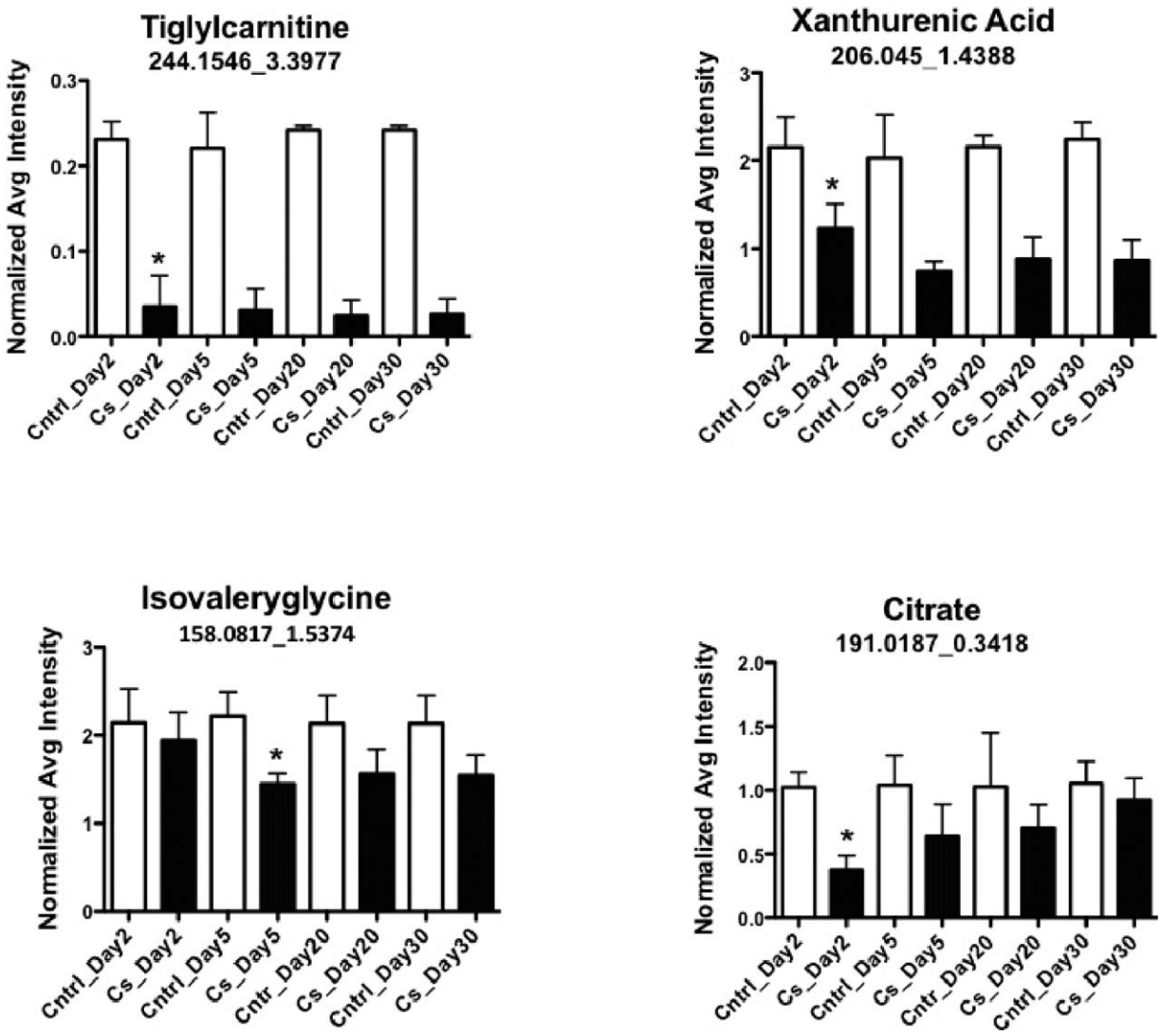

FIG. 4. Urinary excretion abundance of 4 down-regulated metabolite markers in response to ^{137}Cs exposure. Tiglylcarnitine (P value 7.76e^{-7}) and xanthurenic acid (P value 0.0136) were identified in ESI^{+} mode and isovalerylglycine (P value 0.0188) and citrate (P value 0.000478) were found in ESI^{-} mode. The identity of tiglylcarnitine was elucidated based on MS/MS spectra of known carnitine species while the identity of the other 3 metabolites were confirmed by MS/MS. The abundance of each metabolite was normalized to total creatinine and internal standards spiked in urine samples in each ESI mode. *Designates a significant change in the urinary excretion of a metabolite post-irradiation when compared to its urinary excretion in the urine of control mice ($P < 0.05$).

isoleucine and tryptophan metabolic pathways had at least ten metabolites putatively assigned to them (Supplementary Fig. S1; http://dx.doi.org/10.1667/RR13479.1.S1), which indicates considerable perturbations in these pathways due to ^{137}Cs exposure. Citrate and to a lesser extent alpha-ketoglutarate are also down-regulated. Because both of these metabolites are intermediates in the citric acid cycle a decrease in their levels may further indicate a slow-down in energy metabolism.

DISCUSSION

In this study, UPLC-TOFMS provided a platform for exploring the urinary metabolomic signature of ^{137}Cs exposure in mice to determine specific markers of early exposure. This study focused on the most abundant small organic molecules in the urine of mice which could, with potential high accuracy, help predict exposure and shed light on the pathways most perturbed by it. Among such molecules were several of those already noted in γ irradiation studies (external beam) (supplementary material Table S1; http://dx.doi.org/10.1667/RR13479.1.S2). For instance, uric acid, and taurine and isethionic acid both showed significant up-regulation after ^{137}Cs exposure. Uric acid is the enzymatic product of xanthine oxidase, which is coupled to the production of radical moieties. An increase in the urinary excretion of uric acid post ^{137}CsCl injection may indicate an increase in the oxidation of hypoxanthine to xanthine, which subsequently forms uric acid. As a result, more ROS species are produced which can contribute to the

overall radiation-induced ROS injury in mice. The increase in the urinary excretion levels of taurine may be due to its protective role against radiation-induced reactive oxygen species (ROS) damage (*11, 13, 14*). Isethionic acid is taurine's hydroxyl-derivative, and because mammals cannot convert taurine to isethionic acid without the help of the gut microbes (*15*), an increase in its levels post-exposure may be indicative of ^{137}Cs effects on the gut microbial community. Hippuric acid is yet another gut microbiota-mediated metabolite that is excreted after absorption of benzoic acid containing diet and glycine conjugation in liver (*16*). The fivefold increase in the urinary excretion of this metabolite just 2 days post injection (1.95 Gy) also points to the effects of ^{137}Cs exposure on gut microbes. Overall, ^{137}Cs exposure has complicated and persistent effects on the urinary metabolome with substantial overlap with that previously reported by γ irradiation.

Among the statistically significant metabolites are also tiglylglycine (TG) and isovarelyglycine (IVG), both associated with the leucine/isoleucine catabolic pathway. The degradation product of both of these branched-chain amino acids is acetyl-CoA, which ultimately feeds into the TCA cycle (supplementary material Fig. S3; http://dx.doi.org/10.1667/RR13479.1.S1). During the degradation of isoleucine, TG is formed as a byproduct by the mitochondrial enzyme glycine-N-acyltransferase in complex 1 (*17*). An increase in TG's urinary excretion levels is indicative of complex 1 dysfunction as isoleucine is not fully broken down to acetyl-CoA and instead is converted to TG. This also explains the decrease in the urinary excretion levels of isoleucine. It has been shown previously that an X-ray dose of 2 Gy can significantly reduce the efficiency of cardiac mitochondrial complex 1 leading to inefficient respiration and increased oxidative stress in mice (*18*). Thus, an increase in the excretion levels of TG in ^{137}Cs-exposed mice as early as 2 days post-injection (1.95 Gy) may indicate a decrease in the efficiency of complex 1 in converting branched amino acids to acetyl-CoA. IVG and isovaleric acid are two byproducts of leucine degradation to acetyl-CoA and they are formed when there is a deficiency in mitochondrial isovaleric acid-CoA dehydrogenase. The urinary levels of IVG in ^{137}Cs exposed mice decreased as the levels of hydroxyisovaleric acid increased, indicating a shift from a successful degradation of isoleucine to acetyl-CoA to partial breakdown to isovaleric acid. Catabolism of leucine and isoleucine is an important feeder into the TCA cycle. This may explain the significant decrease in the levels of citric acid and alpha-ketoglutarate. A decline in the urinary levels of xanthurenic acid, an intermediate of tryptophan pathway can also explain the lower levels of TCA cycle intermediates as the tryptophan pathway also feeds the TCA cycle. Fatty acid oxidation is another important feeder of the TCA and a decrease in the urinary excretion of two of its members, tiglylcarnitine and hexanoylcarnitine, may also contribute to the decrease in the urinary levels of citric acid. Tiglylcarnitine was found to be down-regulated in the ^{137}Cs exposed mice. Tiglylcarnitine is formed during degradation of isoleucine by the action of mitochondrial enzyme acetoacetyl-CoA thiolase and assists in transporting fatty acids (19). A decrease in its levels may be indicative of deficiencies in mitochondria function. These examples highlight the potential impact of continued exposure to ^{137}Cs on energy metabolism related pathways.

The findings also showed a decrease in body weight of ^{137}Cs-exposed mice compared to control mice (Supplemental Figure 2B), which might be expected with perturbations in energy and microbiome related metabolism. The exposed mice lost 3–10% of their body weight by day 5 post-exposure while the control mice steadily gained weight. The weight of the exposed mice started to increase after the day-5 time point. This is consistent with the levels of some of the mentioned perturbed metabolites whose levels seem to climb at time points 20 and 30 days. The biological effects of ^{137}Cs at the metabolomics level are more severe at earlier days but measurable changes persisted through 30 days post-exposure. The urinary excretion levels of majority of significant metabolites in ^{137}Cs-exposed mice start to resemble those in control mice at days 20 and 30 post-exposure, however, the levels never fully recover. The long-lasting effects of ^{137}Cs exposure thus can be detected even 30 days post exposure as the body adjusts to cope with the effects of ^{137}Cs over time and as magnitude of metabolite changes diminishes. Although there is minimal difference in dose (0.45 Gy) between day 20 and day 30 post-exposure, the effects of ^{137}Cs are persistent and apparent in the levels of metabolites through day 30.

Results with ^{137}Cs address a critical issue for development of biomarkers for human exposure because a variety of potential exposure scenarios involve protracted relatively low-dose rate irradiation, i.e., relative to dose rates used with acute external photon beam exposures. Most radiation stress studies, including others employing metabolomics approaches, have used external-beam irradiation with high dose-rate γ or X rays where the entire dose is delivered in a few minutes (*5, 11, 20*). While the latter may mimic direct irradiation by a nuclear explosion, radiation from internal exposure from radionuclides is continuous and at relatively low-dose rates. In addition, our laboratory and others have found that external-beam irradiation triggers transcriptional responses that are relatively proportional to dose (*21–23*), and the concern arises that continuous protracted irradiation could mimic a series of low doses where molecular responses are at low levels. At some very low level, low dose-rate irradiation would be expected to approach background radiation with no detectable signal. Our current results demonstrate that robust signals at the metabolomics level are generated even though the dose rate averaged only 0.68 mGy/min during the first 2 days and 0.031 mGy/min from 20 to 30 days (supplementary material Table S1; http://dx.doi.org/10.1667/RR13479.1.S2) and gave signals for several metabolites comparable to γ irradiation at 1,670 mG/min (3). For other metabolites (see supplementary

material Table S1) responses were only seen with much higher dose-rate γ irradiation (5) and not with ^{137}Cs. This is reminiscent of radiation responses at the transcriptional level in human cells where many but not all stress-inducible genes showed attenuation at low dose-rate γ irradiation (*23*). In this study, a subset of stress genes showed dose-rate independent responses from 2,900 mGy/min to 2.8 mGy/min. Interestingly, many genes associated with apoptosis showed a dose-rate effect and this correlated with reduced cell killing at low dose rate. Considering that the total absorbed dose over 30 days with ^{137}Cs, 9.91 Gy, appreciably exceeded the $LD_{50/30-}$ (8 Gy) dose for this strain of mice by γ irradiation and that there was no appreciable lethality, a reasonable assumption is that lethality-associated signaling is reduced *in vivo* by low-dose rate exposures and that this may be reflected in some of the differences between ^{137}Cs and γ irradiation. Considering that the urinary metabolome reflects aggregate net changes in metabolites from many tissues as well as the microbiome, the source of signals is probably quite complex. In addition, some metabolite changes were seen after ^{137}Cs but not γ irradiation (supplementary material Table S1; http://dx.doi.org/10.1667/RR13479.1.S2), and this could reflect low-dose rate specific responses or perhaps responses specific for an internal radionuclide. From a biomarker standpoint, measureable metabolite changes were seen up to 30 days after ^{137}Cs injection, and this supports a metabolomics approach to assess radiation exposures.

These findings together with partial degradation of isoleucine/leucine, suggest impairment in mitochondrial efficiency and fatty acid β-oxidation. This is also in accordance with a decrease observed in the urinary abundance of citric acid and α-ketoglutaric acid, which are part of the TCA cycle. Perhaps, monitoring the most affected metabolites can shed light on the long-term effects of ^{137}Cs on mitochondrial function and other important pathways. It will also be interesting to further explore the differences in biological consequences of external-beam irradiation compared to radionuclide poisoning.

CONCLUSION

The results of this study collectively show perturbations in the fatty acid metabolism, amino acid metabolism and the TCA cycle. There are similarities between the urinary metabolomics profile of ^{137}Cs exposed mice and the γ irradiated mice, however, the individual metabolites and the abundances differ between the two types of exposure. Despite relatively low dose-rates compared to previous studies with external-beam γ irradiation, robust responses were seen that for some metabolites increased with time of exposure and hence total absorbed dose in first 3 weeks. Thus, there is ample signal and persistence of signal for radiation biomarkers after exposure to an internal emitter to allow for monitoring of radiation exposures.

ACKNOWLEDGMENTS

This study was supported by the National Institute of Health (National Institute of Allergy and Infectious Diseases) grant U19 A1067773. The authors would like to thank Georgetown University's Radiation Safety Office and the Proteomic and Metabolomics Shared Resources, NIH P30 CA51008, for making the analysis of the radioactive specimens possible. We would also like to acknowledge the efforts of Yue Luo in mass spectrometry analysis and Dr. Evagelia C. Laiakis for her valuable advice, and Drs. Michael Stabin and Luiz Bertelli for calculation of the murine dose coefficients.

Received: July 5, 2013; accepted: October 7, 2013; published online: December 30, 2013

REFERENCES

1. Fushiki S. Radiation hazards in children-Lessons from Chernobyl, Three-mile island and Fukushima. Brain Development 2013; 35:220–227.
2. Boecker BB. Comparison of ^{137}Cs metabolism in the beagle dog following inhalation and intravenous injection. Health Phys 1969; 16:785–788.
3. Stabin MG, Peterson TE, Holburn GE, Emmons MA. Voxel-based mouse and rat models for internal dose calculations. J Nucl Med 2006; 47:655–659.
4. Miller G, Bertelli L, Klare K, Weber W, Doyle-Eisele M, Guilmette R. Software for empirical building of biokinetic models for normal and decorporation-affected data. Health Phys 2012; 103:484–494.
5. Laiakis EC, Hyduke DR, Fornace Jr AJ. Comparison of mouse urinary metabolomics profiles after exposure to the inflammatory stressors gamma radiation and lipopolysaccharide. Radiat Res 2012; 177:187–199.
6. Kanehisa M, Goto S. KEGG: Kyoto encyclopedia of genes and genomes. Nucleic Acids Res 2000; 28:27–30.
7. Zuniga A, Li L. Ultra-high performance liquid chromatography tandem mass spectrometry for comprehensive analysis of urinary acylcarnitines. Anal Chimica Acta 2011; 689:77–84.
8. Chase DH, Hillman SL, Van Hove JLK, Naylor EW. Rapid diagnosis of MCAD deficiency: quantitative analysis of octanoylcarnitine and other acylcarnitines in newborn blood spots by tandem mass spectrometry. Clinical Chem 1997; 43:2106–2113.
9. Millington DS, Roe CR, Maltby DA. Characterization of new diagnostic acylcarnitines in patients with beta-ketothiolase deficiency and glutaric aciduria type I using mass spectrometry. Biomed Environ Mass Spectrom 1987; 14:711–716.
10. Johnson CH, Patterson A, Krausz KW, Lanz C, Kang DW, Luecke H, et al. Radiation metabolomics 4. UPLC-ESI_QTOFMS-based metabolomics for urinary biomarker discovery in gamma-irradiated rats. Radiat Res 2011; 175:473–484.
11. Tyburski JB, Patterson AD, Krausz KW, Slavik J, Fornace AJ, Jr, Gonzalez FJ, et al. Radiation metabolomics 1. Identification of minimally invasive urine biomarkers for gamma-radiation exposure in mice. Radiat Res 2008; 170:1–14.
12. Malina HZ, Richter C, Mehl M, Hess OM. Pathological apoptosis by xanthurenic acid, a tryptophan metabolite: activation of cell caspases but not cytoskeleton breakdown. BMC Physiology 2001; 1:7.
13. Dilley J. The origin of urinary taurine excretion during chronic radiation injury. Radiat Res 1972; 50:191–196.
14. Fellman J, Roth E, Avedovech N, McCarthy K. The metabolism of taurine to isethionate. Arch Biochem Biophys 1980; 204:560–567.
15. Huxtable R, Bressler R. Taurine and isethionic acid: distribution and interconversion in the rat. Nature 1972; 102:805–814.
16. Phipps A, Stewart J, Wright B, Wilson I. Effect of diet on the urinary excretion of hippuric acid and other dietary-derived

aromatics in rat A complex interaction between diet, gut microflora and substrate specificity. Xenobiotica 1998; 28:527–537.

17. Boulange CL, Claus SP, Chou CJ, et al. Early metabolic adaptation in C57BL/6 mice resistant to high fat diet induced weight gain involves and activation of mitochondrial oxidative pathways. J Proteome Res 2013; 12:1956–1968.

18. Barjaktarovic Z, Shyla A, Azimzadeh O, Schulz S, Haagen J, Dorr W, et al. Ionizing radiation induces persistent alterations in the cardiac mitochondrial function of C57BL/6 mice 40weeks after local heart exposure. Radiother Oncol 2013; 106:404–410.

19. Fukao T, Zhang GX, Sakura N, Kubo T, Yamaga H, Hazama A, et al. The mitochondrial acetoacetyl-CoA thiolase (T2) deficiency in Japanese patients: urinary organic acid and blood acylcarnitine profiles under stable conditions have subtle abnormalities in T2-deficient patients with some residual T2 activity. J Inherit Metab Dis 2003; 26:423–431.

20. Tyburski JB, Patterson AD, Krausz KW, Slavik J, Fornace Jr AJ, Gonzalez FJ, et al. Radiation metabolomics 2 dose- and time-dependent urinary excretion of deaminated purines and pyrimidines after sublethal gamma-radiation exposure in mice. Radiat Res 2009; 172:42–57.

21. Amundson SA, Do KT, Fornace Jr AJ. Induction of stress genes by low doses of gamma rays. Radiat Res 1999; 152: 225–231.

22. Amundson SA, Bittner ML, Fornace Jr AJ. Functional genomics as a window on radiation stress signaling. Oncogene 2003; *22*: 5828–5833.

23. Amundson SA, Lee A, Koch-Paiz C, Bittner ML, Meltzer P, Trent J M, et al. Differential responses of stress genes to low dose-rate gamma-irradiation. Mol Cancer Res 2003; 1:445–452.